Available online at www.sciencedirect.com
SCIENCE DIRECT®
Polymer 45 (2004) 2333–2340
polymer
www.elsevier.com/locate/polymer

Enhanced crystallization of bisphenol-A polycarbonate by nano-scale clays in the presence of supercritical carbon dioxide

Xianbo Hu, Alan J. Lesser*

Department of Polymer Science and Engineering, University of Massachusetts, Amherst, Massachusetts, MA 01003, USA

Received 12 August 2003; received in revised form 29 December 2003; accepted 31 December 2003

Abstract

The crystallization behavior of bisphenol-A polycarbonate (PC) and PC/clay nanocomposites were studied in the presence of supercritical carbon dioxide ($SCCO_2$) using DSC, WAXD and AFM. In the absence of $SCCO_2$, nano-scale clay itself does not change the crystallization behavior of PC under our experimental conditions. In the presence of $SCCO_2$, clay appears to be an efficient nucleating agent and enhances the crystallization of PC. The addition of clay reduces the induction time of crystallization and increases the crystallization rate. The increase in crystallinity with clay depends on the crystallization time. When the crystallization time is sufficient, PC and PC/clay composites tend to have similar crystallinity in the range of 26%. Two melting temperatures are observed during the DSC heating scan, and are mainly associated with the melting of both secondary and primary crystals. Results show that the clay influences the primary crystallization process more than the secondary crystallization process.

Keywords: Polycarbonate nanocomposite; Crystallization; Supercritical carbon dioxide

1. Introduction

Previous research has shown that the addition of nano-scale clays into semi-crystalline polymers such poly(trimethylene terephthalate) (PTT) and poly(ethylene terephthalate) (PET) can influence their crystallization behavior. In these systems the change in crystallization behavior depends not only on the type of silicates, but also the crystallization characteristics of the polymer. If the crystallization kinetics of polymer is extremely slow or fast, the influence of the nanosilicate on the crystallization behavior will be more or less effective, respectively [1,2]. Bisphenol-A polycarbonate (PC), therefore, is an ideal candidate for this kind of research since it possesses extremely slow thermal crystallization kinetics. PC undergoes thermal-induced crystallization very slowly because of its chain rigidity, which retards chain diffusion. At 190 °C, one full day is necessary for the first crystallites to develop and a week or more to obtain a well-developed spherulite [3]. The half-time of crystallization, $t_{1/2}$, of PC with a molecular weight higher than 17,000 is more than a week [4,5]. Both solvents [6,7] and vapors [8,9] have been used to induce crystallization in PC. However, due to the high residue of solvents in the crystallized materials as well as the associated environmental considerations, this method is only used in the basic research.

Supercritical carbon dioxide ($SCCO_2$) has been successfully used to crystallize PC thin films at elevated pressures and temperatures [10]. Recently, Stephen G. Gross studied $SCCO_2$ induced crystallization of PCs and the following solid-state polymerization in $SCCO_2$ [11–13]. In this article, crystallization behavior of PC/clay nanocomposites in the presence of $SCCO_2$ is discussed. Crystallization in $SCCO_2$ can overcome the time-consuming process of thermal-induced crystallization as well as the undesirable high residue and environmental issues associated with traditional solvent-induced crystallization.

2. Experimental

2.1. Materials and sample preparation

Two kinds of PC/clay nanocomposites resin pellets (PCL, PCH) and one PC were supplied by US Army Natick

* Corresponding author.
E-mail address: ajl@mail.pse.umass.edu (A.J. Lesser).

0032-3861/$ - see front matter © 2004 Elsevier Ltd. All rights reserved.
doi:10.1016/j.polymer.2003.12.079

Soldier System Center. The PC is Makrolon 2847 (molecular weight: M_w 58,000) resin pellets produced by Bayer Corp. X-ray results indicate that the PCL has an intercalated morphology and PCH has an exfoliated morphology. Both clays are organo-modified montmorillonites. Modifying groups and process methods are proprietary to Triton Systems. The clay concentration in both PCL and PCH systems is 1.5 wt%. The amorphous PC and PC/clay nanocomposites pellets were initially compression molded into 2.5 mm thick sheets. Next, 30 μm thick films were produced using a PHI bench hydraulic melt press at a temperature of 250 °C and a load of 20,000 pounds for 5–15 min. Afterward, the samples were cooled to room temperature by circulating water. Coleman grade carbon dioxide was purchased from Merriam Graves and used as received.

2.2. Crystallization procedure

Crystallization was carried out in a custom high-pressure vessel designed to allow the application of a compressive force to the samples while in the presence of $SCCO_2$. The details of this experimental apparatus have been discussed elsewhere [14]. Samples were conditioned in the vessel without any additional force applied. Sheet specimens and thin films were treated at a fixed temperature and pressure with different times. After crystallization the temperature was allowed to drop and the vessel was depressurized slowly over an 18 h period.

2.3. Characterization

X-ray measurements were conducted on a Siemens D500 diffractometer in transmission mode using a nickel-filtered Cu Kα radiation ($\lambda = 0.154$ nm) operated at 40 kV and 30 mA. Differential scanning calorimetry (DSC) measurements were carried out on a TA Instruments 2910 Modulated DSC (DuPont). Samples were heated from 20 to 260 °C at different scan rates. The degree of crystallinity was calculated using a heat of fusion of 26.2 cal/g for 100% crystalline PC [15]. The crystallinity is normalized with the clay weight percentage. Imaging of thin films was performed with an atomic force microscope (AFM) Dimension-3100 (Digital Instrument, Inc.) in the tapping mode at room temperature. Phase images were collected. Silicon tips with constant number of 40 N/m were used.

3. Results and discussion

3.1. Crystallization behavior

All of the initially transparent specimens became translucent or opaque after the treatment in $SCCO_2$. Polarized optical microscope images of the treated samples indicate the anisotropic structure. In Fig. 1, the untreated PC and PC/clay nanocomposites show only a glass transition during the DSC heating scan. The glass transition temperatures (T_g) of these untreated PC, PCL and PCH are 146, 142 and 138 °C, respectively. After the treatment at 90 °C and 2500 psi in the presence of $SCCO_2$ for 8 h, the DSC results reveal two new endotherm peaks associated with crystal growth. The high melting temperature (T_{m2}) is around 216 °C and the low melting temperature (T_{m1}) occurs at 176 °C. The total crystallinity (X_{ctotal}) of the $SCCO_2$ treated PC (including both endotherms) is only 2.6%. Comparatively, the X_{ctotal} for treated PC/clay nanocomposites is much higher. Those of PCL and PCH are 21.75% and 22.67%, respectively. The evident increase in crystallinity of PC/clay nanocomposites indicates that the addition of nano-scale clays can enhance the crystallization of CP in the presence of $SCCO_2$. When treated in $SCCO_2$ at 3000 psi and 95 °C, the T_{m2} of all the three specimens is still around 217 °C. But the T_{m1} of all samples increases to 184 from 177 °C. However, there is no evident difference in melting temperatures of pure PC and PC/clay nanocomposites. The X_{ctotal} of PC increases to 21.0% with the increase of pressure and temperature. Compared to the treated pure PC, the increase in crystallinity of treated PC/clay nanocomposites is not obvious. Those of PCL and PCH are 25.21% and 24.16%, respectively. Note that both are higher than that of treated PC. All of the DSC data including $T_{m1}, T_{m2}, X_{ctotal}$, and percentage of heat of fusion of the low endotherm peak (X_{c1}) to $X_{ctotal}(X_{c1}/X_{ctotal})$ are summarized in Table 1.

Typical wide-angle X-ray diffraction (WAXD) results are shown in Fig. 2. All untreated samples show one strong, broad reflection at 2θ of 17.6°, and two shoulders at 11° and 25.8°, respectively. Note, however, that PCL has another reflection at 2.9° indicating intercalated morphology. There are no reflection peaks at lower 2θ in the PCH X-ray pattern indicating an exfoliated morphology. Some differences are observed in the X-ray pattern after the treatment in $SCCO_2$. When samples are treated at 90 °C and 2500 psi, the pattern of pure PC appears the same as the untreated material. However, for the PC/clay nanocomposites, the reflection peaks at 17.6° and 25.8° become sharper. These changes in X-ray patterns indicate an increase in crystallinity only in the PC/clay nanocomposites. X-ray results on the samples treated at 95 °C and 3000 psi show a dramatic change similar to that of DSC. After the treatment in these conditions, the reflection peaks at 17.6° and 25.8° for all samples become very sharp and the reflection intensity increases. For the PC/clay nanocomposites, the reflections at 8.9° and 11.7° emerge weak peaks from the shoulders of the untreated samples. These changes in X-ray patterns also indicate the increase in crystallinity. In every case, reflection peaks are at the same position, which match those of Bonart's result [9,16]. This indicates that, although the melting temperatures are different with variant processing conditions, the unit cell of crystal phase in all samples is the same.

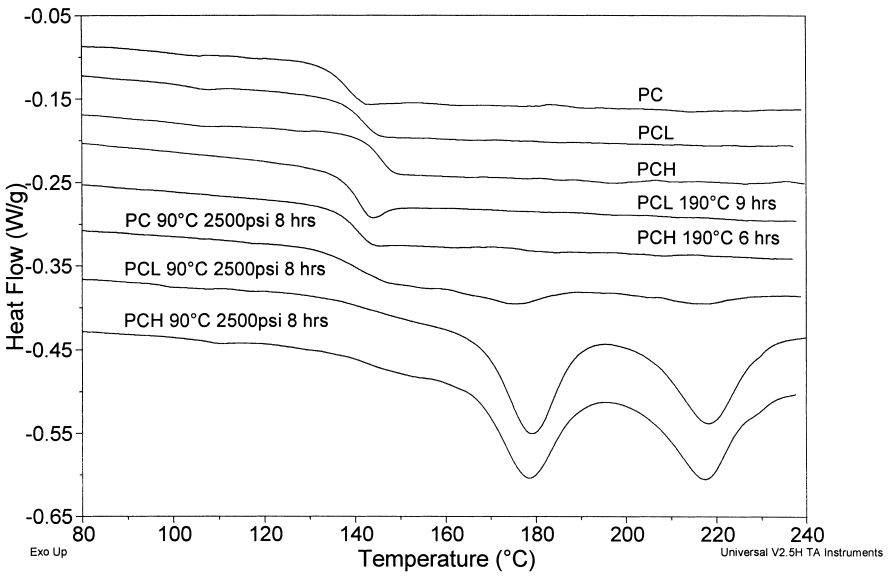

Fig. 1. Typical DSC heating curves of untreated, annealed and CO_2 treated PC, PCL and PCH at 10 °C/min.

The X_{ctotal} vs logarithm of crystallization time t at scan rate 2 °C/min is plotted in Fig. 3. The X_{ctotal} of all samples increases as a function of t. Comparatively, X_{ctotal} of PC/clay nanocomposites are about 5–10% higher. When t is sufficient, PC and PC/clay nanocomposites tend to have similar X_{ctotal} (around 26%). Also there is no evident difference in X_{ctotal} between the PCL and PCH material. From the trend plotted in Fig. 3, it seems that the addition of clay can reduce the induction time of crystallization and increase the crystallization rate. Therefore, the crystallization of PC/clay nanocomposites starts earlier and finishes in a shorter time.

The ratio X_{c1}/X_{ctotal} for PC and PC/clay nanocomposites crystallized at 95 °C and 3000 psi are also plotted in Fig. 3. Note that when the crystallization time is 1 h, the X_{c1}/X_{ctotal} of PC and PC/clay nanocomposites is the same (about 45%). At different times the difference in X_{c1}/X_{ctotal} between PC and PC/clay nanocomposites increases to a maximum and then decreases as a function of time. When the crystallization time is greater than 1 h, the X_{c1}/X_{ctotal} of PC is

Table 1
DSC results of PC and PC/clay composites treated at 95 °C and 3000 psi with different time at various scan rate β

β	PC (h)			PCL (h)			PCH (h)		
	1	3	8	1	3	8	1	3	8
X_{ctotal} (%)									
2	–	4.41	18.26	5.89	19.89	25.57	5.41	19.37	24.79
5	0.77	3.91	18.53	5.98	20.63	21.96	5.84	20.20	18.53
10	2.51	5.59	20.84	10.50	20.70	25.21	5.64	20.33	24.16
20	1.68	5.10	18.65	4.39	21.68	23.51	5.61	17.22	23.77
X_{c1}/X_{ctotal} (%)									
2	–	36.04	41.45	22.11	30.80	32.96	24.04	31.82	32.55
5	–	48.1	52.21	36.53	42.32	43.14	36.50	42.48	42.84
10	44.54	64.38	59.00	45.35	48.94	49.64	45.12	50.53	49.16
20	58.46	85.57	69.61	59.20	62.98	62.42	57.47	66.93	57.24
T_{m1} (°C)									
2	–	176.00	176.64	170.88	175.43	176.40	169.93	174.00	174.80
5	175.4	179.89	181.8	175.2	179.67	181.3	175.2	178.08	181.8
10	174.84	185.29	184.38	179.60	183.61	183.40	178.13	178.21	184.01
20	185.80	187.17	191.39	183.00	188.29	191.02	183.24	188.59	189.17
T_{m2} (°C)									
2	–	220.77	219.40	224.05	223.09	221.98	221.25	221.68	220.88
5	217.2	217.38	217.6	220.3	221.08	220.0	218.4	218.41	217.6
10	215.18	219.76	216.45	220.47	218.94	218.30	217.69	217.60	217.19
20	218.27	217.42	217.19	220.36	219.34	219.40	217.00	218.67	217.93

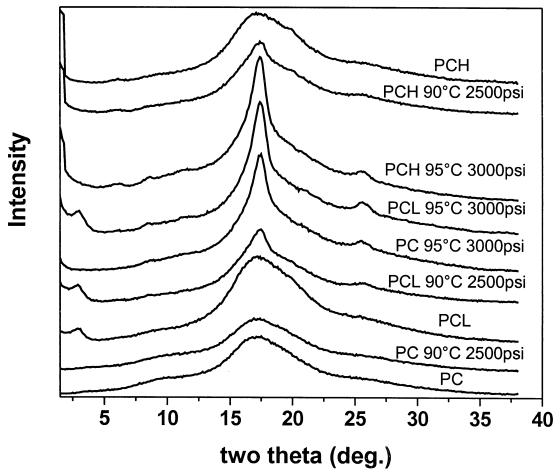

Fig. 2. Typical WAXD results of PC, PCL and PCH treated in CO_2 under different conditions.

higher than those of the PC/clay nanocomposites. For example, when crystallized at 3 and 8 h, X_{c1}/X_{ctotal} of PC is about 15% and 10% higher than those of PC/clay composites, respectively. The decrease in X_{c1}/X_{ctotal} of PC/clay nanocomposites indicates that the addition of about 1.5% of clay decreases the crystalline fraction at T_{m1} and increase the crystalline fraction at T_{m2}.

The influence of $SCCO_2$ on the crystallization of PC has two primary effects. First, although $SCCO_2$ is a non-solvent to most of polymers, it can function as an excellent plasticizer. The significant plasticization results in substantial decrease in the glass transition temperature of polymers [17]. The measured residue of CO_2 in the samples after depressurization is about 3.0–3.5 wt%. According to Chow's model [18], T_gs of PC with 3.0 and 3.5 wt% CO_2 (calculated from with $z = 2$, T_g of PC 145 °C, an average value of $\Delta C_p = 0.0585$ cal/g °C [19]) are 25 and 14 °C, respectively. The extrapolated T_gs of PC to 2500 and 3000 psi from previous research results [20,21] is around −10 °C and −40 °C. Even though the high pressure itself raises T_g by about 5 °C/100 atm [10,22], the T_g in our experiment is definitely much lower than 90 °C since the CO_2 mass uptake should be higher than 3.5% during the treatment. The significant depression in T_g greatly increases the mobility of PC chains and enhances the transport process between the amorphous and crystalline phases. This allows the PC chains to form a more thermodynamically favorable crystalline structure. The T_g depression is a function of CO_2 concentration and, at a constant temperature, it progressively decreases with increasing in pressure. On the other hand, CO_2 can only penetrate amorphous region in semicrystalline polymer, and hydrostatic pressure stabilizes crystal structure. According to Mitsuko [23], $SCCO_2$ increases the crystallization rate at the self-diffusion controlled region and even depresses the crystallization in the nucleation controlled region due to the different depression between the T_g and the T_m.

The T_{max} denotes the temperature at which the crystallization reaches the maximum. T_{max} of PC is around 190 °C and approximately independent of molar mass [4]. T_{max} of PC in 3000 psi CO_2 is around 70–140 °C when the molecular weight of PC is 2500–44,000 g/mol [11,12]. The molecular weight of PC in our research is 58,000 g/mol. Therefore crystallization is mainly controlled by self-diffusion instead of nucleation process in this study. As mentioned before, in the absence of $SCCO_2$, annealing PC even at 190 °C for 24 h did not make it crystallize. Thus, $SCCO_2$ enhances the crystallization of PC significantly.

3.2. Melting behavior

DSC results also show the different dependence of T_{m2} and T_{m1} on crystallization time t. T_{m2} is independent of t. T_{m2} of PC and PC/clay composites are almost the same, about 219 ± 2 °C, seen in Table 1. There is no obvious difference among them and T_{m1} increases with t. As shown in Fig. 4, the difference in T_{m1} of samples crystallized at

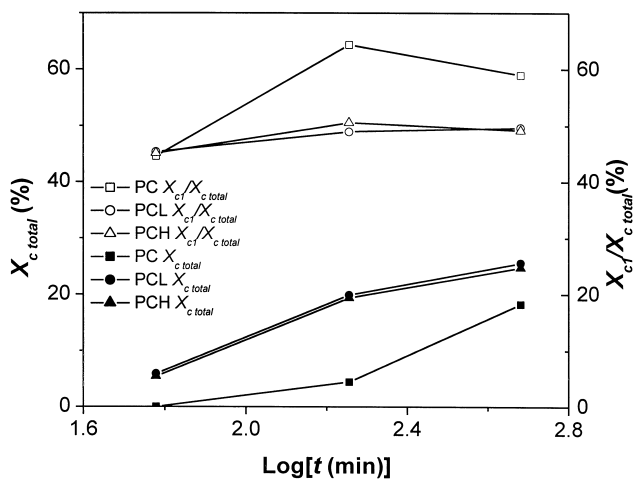

Fig. 3. Plots of X_{c1}/X_{ctotal} and X_{ctotal} > vs log t of PC, PC/clay composites crystallized at 95 °C 3000 psi.

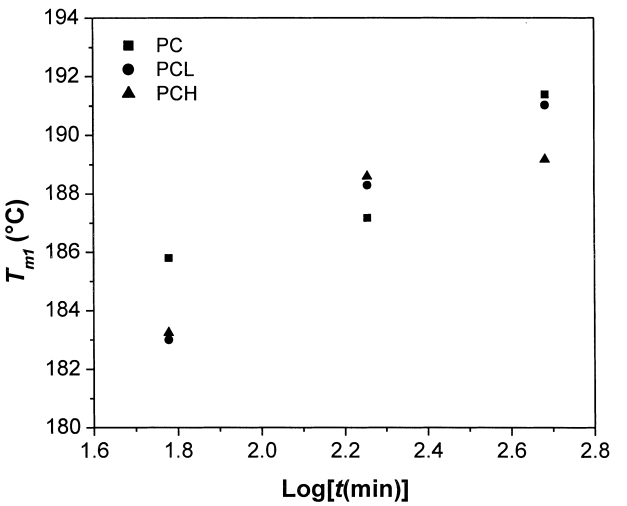

Fig. 4. Plots of T_{m1} vs log t of PC, PCL and PCH crystallized at 95 °C 3000 psi with different time with a scan rate of 20 °C/min.

95 °C and 3000 psi at various times is about 6–8 °C. PC and PC/clay nanocomposites show the similar trend. The influence of t on T_{m1} is similar to that of CO_2 pressure on T_{m1}.

As shown in X-ray results, the two T_ms are not the result of different unit cells. Thus the two T_ms and the difference in T_m at different conditions occur for other reasons. T_{m1}s are plotted with the square root of scan rate $\beta^{1/2}$ in Fig. 5. Note that an increase in scan rate leads to an upward shift of T_{m1} obviously. T_{m1}s are well described by a linear function of $\beta^{1/2}$. K (the slope of the various T_m1 vs $\beta^{1/2}$ line) is in the range of 3.6–5.0. This indicates that the crystals related to T_{m1} show a superheating behavior. In polymers, two types of crystal structure can result in this kind of superheating [24]. The first includes extended chain crystals such as those found in polyethylene or polytetrafluoroethylene. Superheating is due to the slow kinetics of melting large crystals. The second includes meta-stable crystals with conformationally constrained interfacial chains, such as tie chains or loose loops that exhibit reduced entropy of fusion upon melting.

According to S. Sohn [25], a constant value for the slope of T_{m1} vs $\beta^{1/2}$ is incompatible with the concept of a multiple melting behavior by a melting–recrystallization–remelting process. Thus, T_{m1} is not associated with the difference in crystal perfection, lateral dimensions or thickness. Rather it is a consequence of a decrease in molar conformational entropy of the remaining amorphous fraction, which results in secondary crystallization. T_{m2} is associated with melting of primary crystals. If this hypothesis is true, the heat of fusion of first and the second endotherm peaks should be associated with crystallinity of secondary and primary crystals. Also, X_{c1}, should represent the crystallinity of second crystallization process and have a similar dependence on β as T_{m1}. This is shown clearly (Fig. 6) to be the case with X_{c1}/X_{ctotal} also having a linear function with $\beta^{1/2}$.

Since T_{m2} is related to melting of lamellae formed during the primary crystallization process, it should depend not on the β but only on the thickness or perfection of the crystallites. This is also true when β is in certain range. T_{m2}s are plotted with the square root of scan rate $\beta^{1/2}$ in Fig. 7. Also, when β is in the range of 5–20 °C/min, the increase in scan rate has no obvious effect on the higher melt temperature and T_{m2}s are around 219 ± 2 °C. When β is 2 °C/min, the T_{m2}s are around 222 ± 2 °C. It seems that T_{m2} increases with decrease in β, especially when the scan rate is very low. The fact that T_{m2} increases with a decrease in β means there is still a small fraction of melting–recrystallization–remelting process occurring during the DSC heating scan, especially when the scan rate is very low. But this influence is neglectable due to the high rigidity of PC chain. Overall, the two melting temperatures T_{m1} and T_{m2} observed during the DSC heating scan are associated with the melting of secondary and primary crystals, respectively.

The atomic force microscope (AFM) analyses also

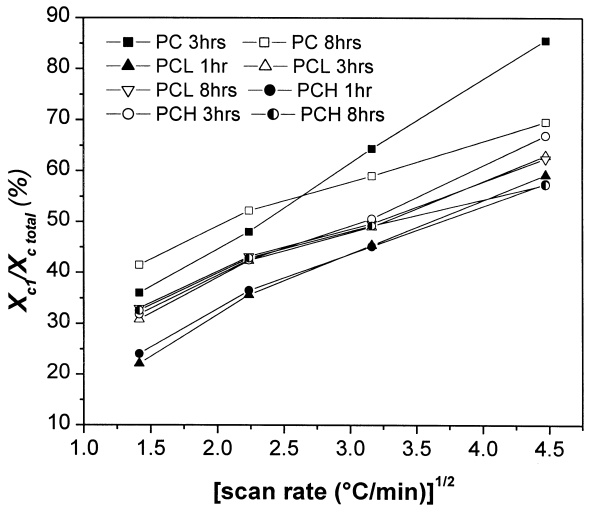

Fig. 6. Plots of X_{c1}/X_{ctotal} vs square root of scan rate $\beta^{1/2}$ of PC, PCL and PCH at 95 °C and 3000 psi with different times.

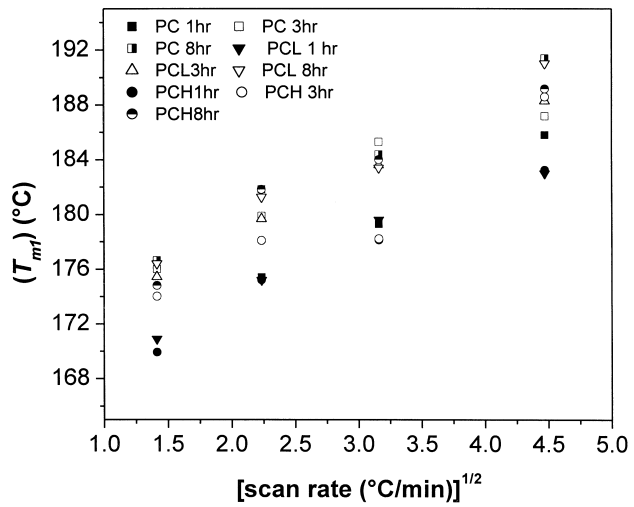

Fig. 5. Plots of T_{m1} vs square root of scan rate $\beta^{1/2}$ of PC, PCL and PCH at 95 °C and 3000 psi with different times.

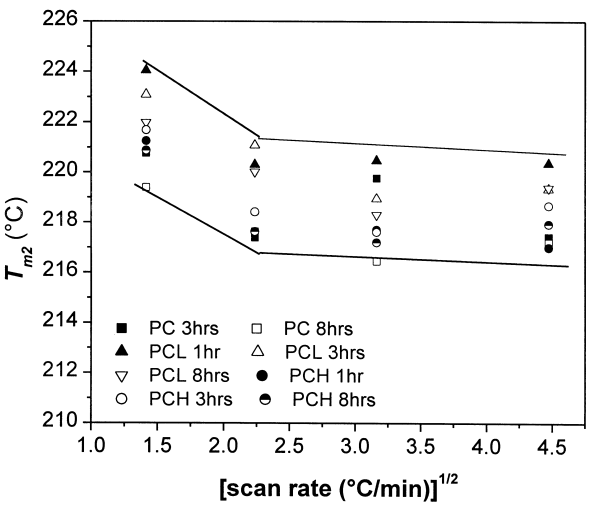

Fig. 7. Plots of T_{m2} vs square root of scan rate $\beta^{1/2}$ of PC, PCL and PCH at 95 °C and 3000 psi with different times.

support the above hypothesis. Fig. 8 shows the AFM phase images of amorphous PC, $SCCO_2$ treated PC and PC/clay nanocomposites (at 95 °C and 3000 psi for 8 h). Currently, phase imaging by AFM is a popular technique for spatially imaging compositional differences between polymer phases or multi-component materials. It is generally accepted that observed phase changes relate to the energy dissipated by the oscillating probe in the sample. Any difference in elastic moduli, viscoelasticity, and/or adhesion will result in a contrast in phase behavior. Normally, the stiffer, less dissipative material is associated with lighter colors in the phase image. Consequently, the lighter regions in Fig. 8 correlate with the crystalline phase, and the darker regions are associated with the amorphous phase.

Note that the crystal morphology is very different from those observed from solvent-induced [4,26] or even thermal-induced crystallization [27]. In those studies spherulitic structures and round-shaped patterns of 30–50 nm diameter in substructure of spherulite were observed. However, no spherulites were found during the crystallization in $SCCO_2$. In all samples, the main components are numerous fibrillar nanocrystallites associated with lamellar growth. Also note that each fibril consists of several lamellae and the width of the fibrillar crystals is around 40–120 nm depending upon crystallization conditions. The lamellar thickness is around 8–12 nm, which is in the same range of that crystallized from solvent [4]. But the lamellae are much shorter in length. There is also complex branching, twisting, and stacking among these lamellae as well as separated lamellae. It is reasonable to propose that the huge amount of these highly dense and complex fibrillar crystal structures produce a high fraction interfacial phase or secondary crystal structure with lower conformational entropy. This is consistent with our DSC results that X_{c1}/X_{ctotal}, the percent of the secondary crystallization of PC and PC/clay nanocomposites are indeed very high (about 62% and 50%, respectively). Previous research strongly suggests that the low melting peak in many semi-crystalline polymers is associated with the melting of bundle-like or fringed micellar crystal morphologies [21,28–30].

Also, the shift in T_g after treatment in $SCCO_2$ supports this point as well. The T_g of untreated PC, PCL and PCH

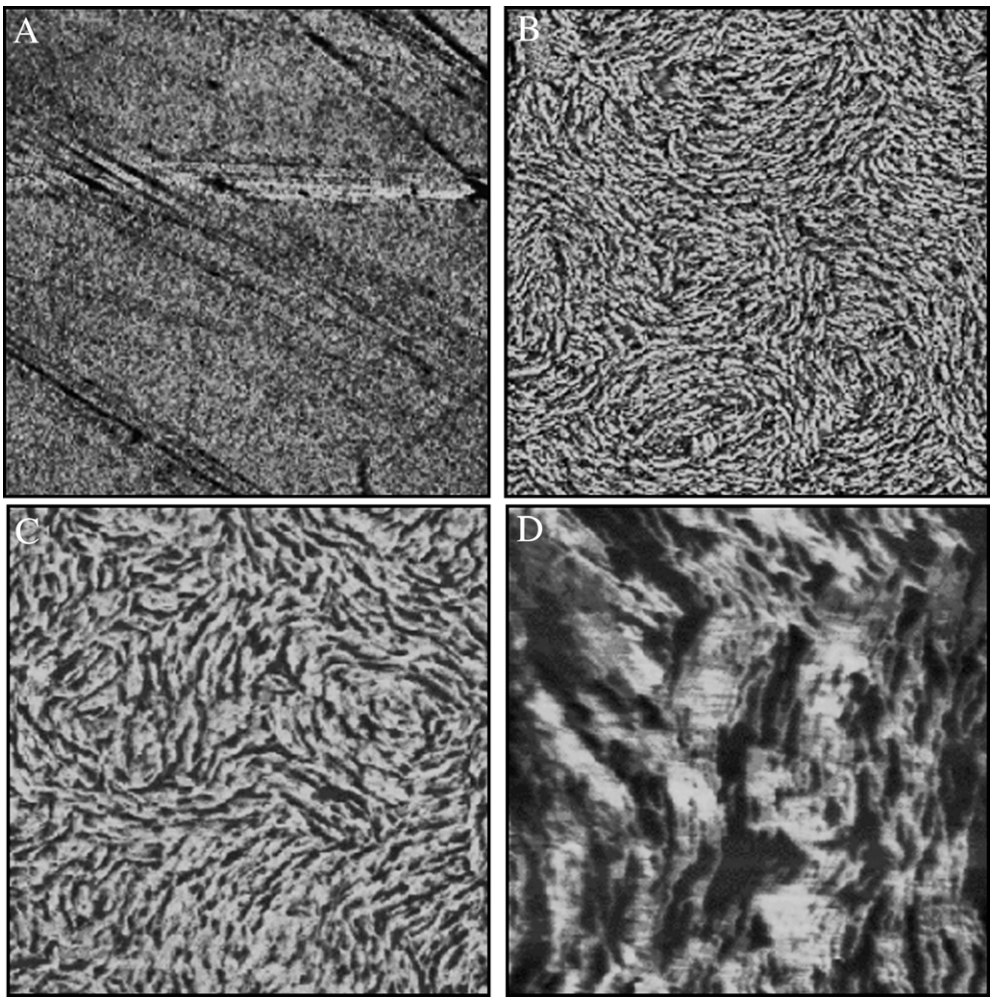

Fig. 8. AFM phase images of pure PC, PC and PCH crystallized at 95 °C and 3000 psi for 8 h. (A): pure PC 5 × 5 μm; (B): crystallized PC 5 × 5 μm; (C): crystallized PCH 5 × 5 μm; (D): crystallized PCH 1 × 1 μm.

(Fig. 1) are 146, 142 and 138 °C, respectively. After treatment (90 °C and 2500 psi for 8 h), the T_g of PC, PCL and PCH are 140.7, 144.5 and 142.4 °C, respectively. The increase in T_g together with the increased X_{ctotal} of PC/clay nanocomposites indicate that the numerous fibrillar micro-crystals increase the degree of conformational constraints on the PC chains.

The increase in crystallization time and CO_2 pressure will decreases the conformational entropy of the secondary crystals and neighboring amorphous fraction. Thus, the T_{m1}s of samples increase as a function of crystallization time and CO_2 pressure. K in Fig. 5 is around 3.6–5.0, which is much higher than those of PC (1.52) and syndiotactic 1,2-polybutadiene (1.63) [25,31]. It seems that the smaller dimension of the fibrils, the higher percent of secondary crystallization are the reasons for the higher slope of T_{m1} vs $\beta^{1/2}$.

3.3. Effect of nano-scale clay

As mentioned in the introduction section, the addition of nano-scale additives can significantly change the crystallization behavior of polymers such as PTT [2], nylon 6 [32] and PP [33]. In order to investigate this type of effect, the PCL and PCH were annealed at 190 °C without CO_2 for 9 and 6 h, respectively. As seen in Fig. 1, there is no endotherm peak indicating melting of any crystal structures. The endotherm following the T_g for PCL is attributed to the physical aging or annealing of any polymer containing a reasonable amount of amorphous content [34]. Since the focus of this contribution is on the crystallization behavior of PC/clay nanocomposites in the presence of $SCCO_2$, annealing for longer times (e.g. for around 54 h [4]) have not been carried out. This result indicates clay itself does not change the crystallization behavior of PC without CO_2 under our experimental conditions.

It seems that so far under our experimental conditions nano-clay itself does not change the crystallization behavior of PC in the absence of CO_2. But the higher crystallinity of PC/clay nanocomposites both from DSC and X-ray results indicate apparently that the addition of nano-scale clays into PC can enhance the crystallization of PC in the presence of $SCCO_2$. This suggests a certain kind of synergism occurs when clay and $SCCO_2$ are combined.

The influence of the clays is observed in several respects. First, the addition of clay reduces the induction time of crystallization and increases the crystallization rate. Therefore, the crystallization of PC/clay nanocomposites starts earlier and finishes in a shorter time. Under most of our experimental conditions, the addition of clay increases the crystallinity of PC. However, it seems that the clays have no obvious increase in the final crystallinity of PC if both the PC and PC/clay nanocomposites are given enough time to fully crystallize. Secondly, the decrease in X_{c1}/X_{ctotal} of PC/clay composites indicates that the addition of about 1.5% of clay increases the primary crystallization or reduces the secondary crystallization. The percent of secondary crystallization, X_{c1}/X_{ctotal} of pure PC is about 10% higher than those of PC/clay nanocomposites. This can also be seen quantitatively from the AFM images, where the size of fibrillar crystallites of PC/clay is larger than that of pure PC. And finally, it appears that (Fig. 7), at given scan rate and identical crystallization condition, the T_{m2} of PC is about 2 and 4 °C lower than those of PCH and PCL, respectively. This increase in T_{m2} indicates that clay is helpful in the formation of crystals with fewer defects. From the above discussion, we conclude that the nano-scale clay is still an efficient nucleating agent and can enhance the crystallization of PC in the presence of $SCCO_2$. Also influence of clays is more dominant in the primary crystallization process than in the secondary crystallization process. There is also no obvious difference between the crystallization between the two types of PC/clay nanocomposites. This is somewhat surprising given the fact that PCL and PCH have different initial morphologies (intercalated vs exfoliated). One might expect for example, that the exfoliated PCH would have more nucleating surface area than the PCL, and, therefore, have faster crystallization kinetics than that of the PCL. The reason for this is not observed is not fully understood. A possible explanation may lie in the different types of clay modifiers used, which may develop different surface energies. This, in turn, may result in a different nucleating activity. Other research on poly(trimethylene terephthalate)/clay systems indicate that a modified-clay can have a higher nucleating activity than an unmodified system [35]. Also, the crystallization kinetics is a result of the entire crystallization procedure, which includes both the nucleation and growth process. One possibility is that the exfoliated PCH may have more nuclei than intercalated PCL, but the crystallites in PCL may be larger than those in PCH. Therefore, there is no evident difference in the crystallinity between PCL and PCH. Again, similar phenomenon was also observed in our PTT/clay system. In that case, the crystallization activation energy increases as a function of clay concentration, but the crystallization rate, nucleating activity still increase with the increase in clay concentration [35].

Now we can propose a procedure crystallization procedure for PC/clay nanocomposites in the presence of $SCCO_2$. The growth process is very difficult due to the high rigidity of PC chain. In the absence of CO_2, although a number of dispersed clays can act as a nucleation agent, the extremely slow diffusion of polymer makes crystallization impossible. In the presence of $SCCO_2$, highly efficient plasticization occurs combined with the nucleating effect from nano-scale clay, to result in a greatly enhanced crystallization process. It may be possible that the great stiffness of PC chains increases the tendency of lamellae to grow closely together from the origin of the nuclei (such as clay surface). There may be also aggregation of neighboring chains instead of chain folding through a reptation tube [36]. Both will result in a fibrillar crystal morphology. Furthermore,

the high chain rigidity of PC may lead to a reduced frequency of adjacent reentries folding and higher occurrence of penetration between lamellae. A similar process happens to the interfaces in interfibrillar regions. Chain segments pinned in interlamellar and interfibrillar regions are therefore are highly constrained. This confinement may result in high fraction of polymer chains in interlamellar and interfibrillar regions compared to flexible crystallizable polymers such as polyethylene, which mainly undergo chain-folding during crystallization.

4. Conclusion

In the absence of CO_2, clay itself does not change the crystallization behavior of PC under our experimental conditions. In the presence of CO_2, the nano-scale clay is still an efficient nucleating agent and enhances the crystallization of PC. The addition of clay can reduce the induction time of crystallization and increase the crystallization rate. The increase in crystallinity with clay depends on the crystallization time. When the crystallization time is long enough, PC and PC/clay composites tend to have similar crystallinity, about 26%. The two melting temperatures of PC during the DSC heating scan of are mainly associated with the melting of secondary and primary crystals. The low melting temperature increases with the increase in crystallization time, CO_2 pressure. The influence of clay on the crystallization of PC is much more dominant in the primary crystallization process than in the secondary crystallization process. There is not obvious difference in the crystallization between the two kinds of PC/clay nanocomposites.

Acknowledgements

The authors wish to thank the Materials Science and Engineering Center (MRSEC) UMASS and the Army Research Laboratory for financial support.

References

[1] Ke YC, Long CF, Qi ZN. J Appl Polym Sci 1999;71:1139–46.
[2] Hu XB, Lesser AJ. J Polym Sci, Polym Phys 2003;41(19):2275–89.
[3] Vonfalka B, Rellensman W. Makromolekulare Chemie 1965;75:122.
[4] Alizadeh A, Sohn S, Quinn J, Marand H, Shank LC, Iler HD. Macromolecules 2001;34:4066–78.
[5] Vonfalka B, Rellensman W. Makromol Chem 1965;88:38.
[6] MacNulty B. J Polym 1968;9:41–4.
[7] Kambour RP, Gruner CL, Romagosa EE. Macromolecules 1974;7:248–53.
[8] Mercier JP, Groeninckx G, Lesne M. J Polym Symp 1967;16:2059–67.
[9] Jonza JM, Porter RS. J Polym Sci Part B: Polym Phys 1986;24:2459–72.
[10] Beckman E, Porter RS. J Polym Sci Part B: Polym Phys 1987;25:1511–7.
[11] Gross SM, Flowers D, Roberts G, Kiserow DJ, DeSimone JM. Macromolecules 1999;32:3167–9.
[12] Gross SM, Roberts G, Kiserow DJ, DeSimone JM. Macromolecules 2000;33:40–5.
[13] Gross SM, Roberts G, Kiserow DJ, DeSimone JM. Macromolecules 2001;34:3916–20.
[14] Caskey TC, Lesser AJ, McCarthy TJ. J Polym Engng Sci 2001;84:134.
[15] Mercier JP, Legras R. J Polym Sci Part B: Polym Lett 1970;8:645–50.
[16] Bonart R. Makromol Chem 1966;92:149.
[17] Chiou JS, Barlow JW, Paul DR. J Appl Polym Sci 1985;30:2633–42.
[18] Chow TS. Macromolecules 1980;13:362–4.
[19] Mathot VBF. Polymer 1984;25:579–99.
[20] Zhang ZY, Handa YP. J Polym Sci Part B: Polym Phys 1998;36:977–82.
[21] Alessi P, Cortesi A, Kikic I, Vecchione F. J Appl Polym Sci 2003;88:2189–93.
[22] Zoller P, Hoehn HH. J Polym Sci, Polym Phys Ed 1982;20:1385–97.
[23] Takada M, Ohshima M. Polym Engng Sci 2003;43:479–89.
[24] Wunderlich B, Macromolecular physics, vol. 3. New York: Academic Press; 1976.
[25] Sohn S, Alizadeh A, Marand H. Polymer 2000;41:8879–86.
[26] Harron HR, Pritchard RG, Cope BC, Goddard DT. J Polym Sci Part B: Polym Phys 1996;34:173–80.
[27] Magonov SN, Kempf S, Kimmig M, Cantow HJ. Polym Bull 1991;26:715–22.
[28] Zachmann HG, Peterlin A. J Macromol Phys 1969;B3:495.
[29] Alizadeh A, Richardson L, Xu J, McCartney S, Marand H, Cheung YW, Chum S. Macromolecules 1999;32:6221–35.
[30] Marand H, Alizadeh A, Farmer R, Desai R, Velikov V. Macromolecules 2000;33:3392–403.
[31] Sasaki T, Sunago H, Hoshikawa T. Polym Engng Sci 2003;43:629–38.
[32] Wu TM, Liao CS. Macromol Chem Phys 2000;201:2820–5.
[33] Assouline E, Lustiger A, Barber AH, Cooper CA, Klein E, Wachtel E, Wagner HD. J Polym Sci Part B: Polym Phys 2003;41:520–7.
[34] Orreindy SA, Rincon G. J Appl Polym Sci 1999;74:1646–8.
[35] Hu XB, Lesser AJ. Macromol Chem Phys 2004; in press.
[36] Hong PD, Chung WT, Hsu CF. Polymer 2002;43:3335–43.